Available online at www.sciencedirect.com

SciVerse ScienceDirect

Procedia Engineering 55 (2013) 165 – 170

Procedia Engineering

www.elsevier.com/locate/procedia

6th International Conference on Creep, Fatigue and Creep-Fatigue Interaction [CF-6]

Analysis of Hysteresis Loops of 316L(N) Stainless Steel under Low Cycle Fatigue Loading Conditions

Samir Chandra Roy[a], Sunil Goyal[b*], R. Sandhya[b], S. K. Ray[a]

[a]*Metallurgical and Material Engineering, Jadavpur University, Kolkata- 700 032, India*
[b]*Indira Gandhi Centre for Atomic Research, Kalpakkam- 603 102, India*

Abstract

Low cycle fatigue tests were carried out on 316 L(N) stainless steel at room temperature employing strain amplitudes ranging from ± 0.3 to ±1.0 % and a strain rate of $3\times10^{-3}s^{-1}$. The material showed initial hardening for a few cycles followed by prolonged softening, saturation and final failure. The fatigue life was found to decrease with increase in strain amplitude. The analysis of stable hysteresis loops showed non-Masing behaviour for this material. The elasto-plastic response of the material under cyclic loading was characterized taking into account isotropic and kinematic hardening occurring during cycling. The material parameters were obtained from the experimental hysteresis loops and cyclic stress response of the material. Finite element analysis of elasto-plastic deformation was carried out to obtain the stabilized hysteresis loop and cyclic stress response of the material. The predicted hysteresis loops showed good agreement with experimental results. The low cycle fatigue life prediction was carried out based on plastic strain energy dissipation with cycling.

Keywords: Low cycle fatigue; non-Masing behavior; isotropic hardening; kinematic hardening; plastic strain energy dissipation.

1. Introduction

In liquid metal cooled fast breeder reactors (LMFBRs), the components are often subjected to repeated cyclic thermal stresses as a result of temperature gradients which occur during start-ups and shut-downs or during transients. Therefore, low cycle fatigue (LCF) represents a predominant failure mode, requiring significant consideration in the design and life analysis of LMFBR components [1, 2]. The material may exhibit Masing or non-Masing behavior under fatigue loading depending on the microstructure and experimental conditions. For materials showing Masing behavior, the matching of compressive tips of the hysteresis loops coincide with the cyclic stress-strain curve magnified by two. Whereas, for materials that show non-Masing behavior, coincidence occurs only when the saturated hysteresis loops are translated along the linear elastic slope to match the loading branches [3-7].

* *Corresponding Author:*
E-mail address: goyal@igcar.gov.in

doi:10.1016/j.proeng.2013.03.237

For accurate LCF life prediction using hysteresis loop energy, it is very important to predict the hysteresis loop accurately. The prediction of hysteresis loop depends on the hardening models that characterize the hysteresis loop. Among the various hardening models available in literature [8] the most widely used are Armstrong and Frederick for non-linear kinematic hardening. In the present investigation, the analysis of hysteresis loop energy is used for the low cycle fatigue life prediction. The saturated hysteresis loops obtained from experiments are compared with the hysteresis loops predicted with finite element analysis by incorporating the combined kinematic and isotropic hardening. The low cycle fatigue life is predicted based on non-Masing analysis of stabilized hysteresis loops obtained at various strain amplitudes in experiments.

2. Experimental

316L(N) SS material used in the present study has the following chemical composition (in wt.%): C: 0.027, Mn: 1.7, Ni: 12.2, Cr: 17.53, Mo: 2.49, N: 0.07, Si: 0.22, S: 0.0055, P: 0.013, Fe: balance. The material was subjected to a solution annealing treatment at 1373 K for 1 h followed by water quenching. LCF experiments were carried out on cylindrical specimens of gauge length 25 mm and diameter 10 mm employing a constant strain rate of 3×10^{-3} s^{-1} at different strain amplitudes (± 0.30 % to ± 1.0 %) at room temperature. All the tests were carried out in air under fully reversed, total axial strain control mode employing a symmetrical triangular strain-time waveform using DARTEC servo hydraulic fatigue testing system.

3. Computations

Finite element analysis (FEA) of low cycle fatigue behavior was carried out using ABAQUS finite element software. The elasto-plastic response of the material under low cycle fatigue loading was modeled using combined nonlinear kinematic and exponential isotropic hardening laws [9].

In case of nonlinear kinematic hardening, the back stress (x) is defined by the following expression:

$$x = \frac{c}{\gamma}\left(1 - e^{-\gamma\varepsilon^p}\right) \tag{1}$$

where ε^p is plastic strain, γ and c are the kinematic hardening material constants and γ determines the rate at which the saturation of back stress c/γ is reached. Kinematic hardening coefficients were obtained from the experimental tensile part of saturated hysteresis loops obtained from experiments.

In case of isotropic hardening, the isotropic function ($r(p)$) is defined by the following equation,

$$r(p) = Q\left(1 - e^{-bp}\right) \tag{2}$$

in which p is accumulated plastic strain, b and Q are material constants and b determines the rate at which $r(p)$ reaches saturation (Q). Isotropic hardening coefficients were obtained from the stress-strain hysteresis loop of experimental data.

4. Results and discussions

4.1. Cyclic stress response

The dependency of peak tensile stress on number of cycles and strain amplitude is depicted in Fig. 1. The material showed initial hardening followed by gradual prolonged softening, saturation and final failure.

The cyclic stress-strain curve and the variation of low cycle fatigue life with total, elastic and plastic strain amplitudes is represented by the following relationship respectively:

$$\Delta\sigma/2 = K'\left(\Delta\varepsilon_p/2\right)^{n'} \quad (3)$$

$$\frac{\Delta\varepsilon_t}{2} = \frac{\sigma'_f}{E}\left(2N_f\right)^b + \varepsilon'_f\left(2N_f\right)^c \quad (4)$$

Where $\Delta\sigma$, $\Delta\varepsilon_p$, $\Delta\varepsilon_t$, N_f, E, K', n', σ_f', b, ε_f', c are stress range, strain range, total strain range, no of cycle to failure, Young's modulus, cyclic strength coefficient, cyclic strain hardening exponent, fatigue strength coefficient, fatigue strength exponent, fatigue ductility coefficient and fatigue ductility exponent respectively. LCF parameters obtained from experimental data are shown in Table 1.

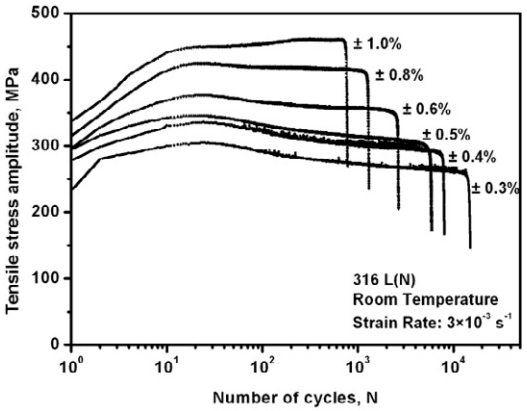

Fig. 1. Cyclic stress response curve of 316 L(N) SS.

Table. 1. Values of coefficients of strain-life relation for 316 L(N) SS

Cyclic stress strain curve coefficients		Basquin relation coefficients		Coffin-Manson relation coefficients	
K'	n'	σ_f'	b	ε_f'	c
2854 MPa	0.378	1444 MPa	-0.159	0.294	-0.494

4.2. Comparison of cyclic behaviour

Combined isotropic and kinematic hardening model was employed in cyclic elasto-plastic finite element analysis to predict the hysteresis loop and cyclic stress response of the material, Table 2.

Table. 2. Elastic and hardening properties of 316 L(N)

Young's Modulus	Yield stress	Kinematic hardening parameters		Isotropic hardening parameters	
E: 200 GPa	σ_0: 211 MPa	C: 57805 MPa	γ: 619.04	Q: 42.30 MPa	b: 21.60

The coefficients were obtained from the experimental hysteresis loops at a total strain amplitude ± 0.5 % and were incorporated in the material model defined in FEA. Fig. 2 and Fig. 3 show the comparison of the simulated hysteresis loop obtained from ABAQUS and experimental for ± 0.4 % and ± 0.5 % strain amplitudes respectively. The results showed good agreement between the numerical simulation and the experimental results. However, at higher strain amplitudes the extent of hardening was lower in simulated first cycle.

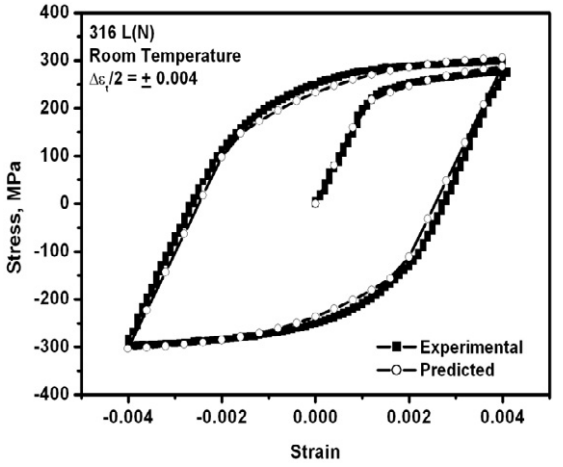

Fig. 2. Comparison of first cycle hysteresis loop obtained from experiment and simulation, ± 0.4 % strain amplitude

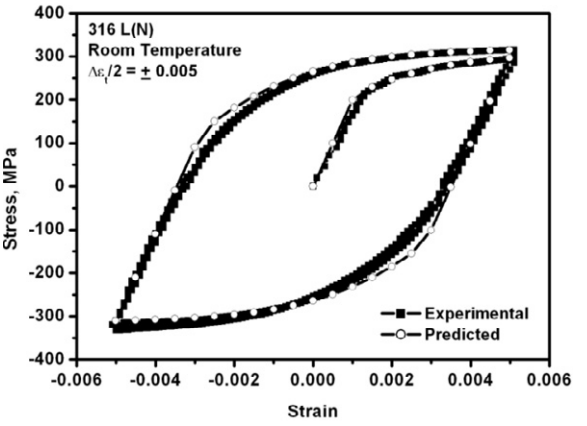

Fig. 3. Comparison of first cycle hysteresis loop obtained from experiment and simulation, ± 0.5 % strain amplitude.

Initial few cycles were predicted by finite element analysis. Fig. 4 and Fig. 5 show the comparison of the tensile stress amplitude with number of cycles for experiments and simulation at strain amplitudes of ± 0.4 % and ± 0.5 % respectively.

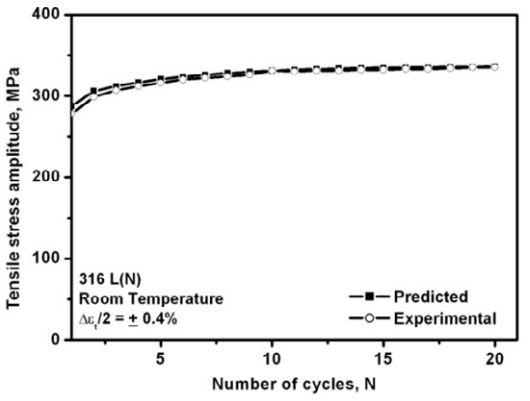

Fig. 4. Comparison of cyclic stress response from experiment and simulation, ± 0.4% strain amplitude.

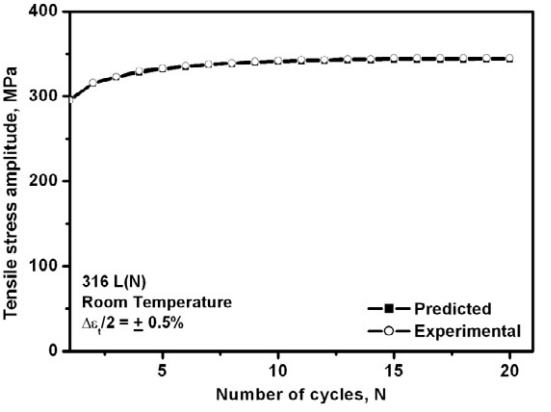

Fig. 5. Comparison of cyclic stress response from experiment and simulation, ± 0.5% strain amplitude.

Good correlation was obtained between the responses simulated using the determined parameters and the experimental observations. However, higher cyclic stress response obtained from experiments than by simulation could be due to non-Masing behavior exhibited by the material above ±0.5% strain amplitude.

4.3. Hysteresis loop analysis and fatigue life prediction

The cyclic stress response showed the saturation after few cycles as shown in the Fig. 1. Saturated hysteresis loops with common compressive tips for various strain amplitudes are plotted in Fig. 6.

The figure shows that loading part of the saturated hysteresis loops follow the common loading curve, representing the Masing behavior [3] at low strain amplitudes (± 0.3 % to ± 0.5 %). At higher strain amplitudes (± 0.6 % to ± 1.0 %), saturated hysteresis loops do not follow the common loading curve and depicts the non-Masing behavior [4]. Detailed microstructural investigation of 304LN SS carried out by Sivaprasad et al. showed that the non-Masing in the material was due to the phase instability and transient dislocation substructure [6].

In order to determine the total plastic strain energy dissipated till failure, accurate measurement of hysteresis loops and cyclic properties of the material is essential. To calculate the hysteresis loop area, a Master curve is generated for stable hysteresis loops at different strain amplitudes. The Master curve is obtained by matching the loading branches of stable hysteresis loops of different strain amplitudes and by translating each loop along the linear elastic portions as shown in Fig. 7.

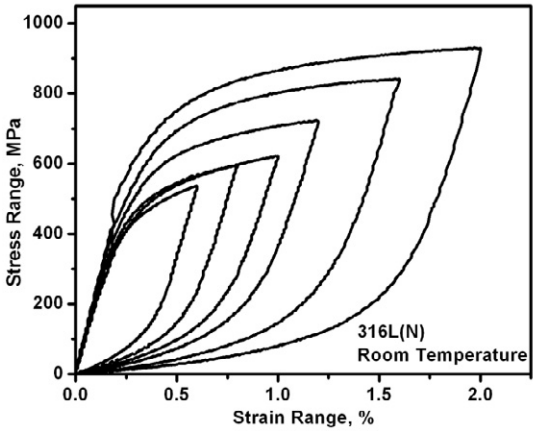

Fig. 6. Stable hysteresis loops common compressive tips.

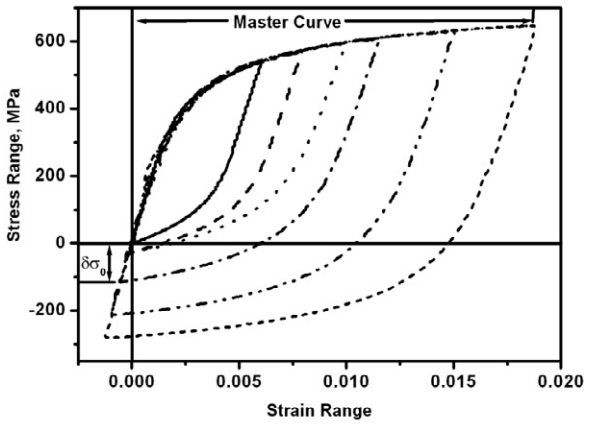

Fig. 7. Construction of Master curve for non-Masing analysis.

The total strain energy released during fatigue (W_T) is calculated by multiplication of no of cycles to failure (N_f) and area under the stable hysteresis loop (ΔW), Eq. (5) [3, 6].

$$W_T = \Delta W . N_f \tag{5}$$

$$\Delta W = \left(\frac{1-n}{1+n}\right)\Delta\sigma.\Delta\varepsilon_p + \left(\frac{2n}{1+n}\right)\delta\sigma_0.\Delta\varepsilon_p \tag{6}$$

where n is the strain hardening exponent of Master curve, $\delta\sigma_0$ is the change in proportional limit of stable loops for different strain amplitude.

In case of Masing behaviour the second term of Eq. (6) is to be omitted and n was found to be different for Masing and non-Masing behavior. Parameter n obtained from the Master curve was found to be 0.152. The predicted fatigue life shows good agreement with the experimental fatigue lives, as shown in Fig. 8.

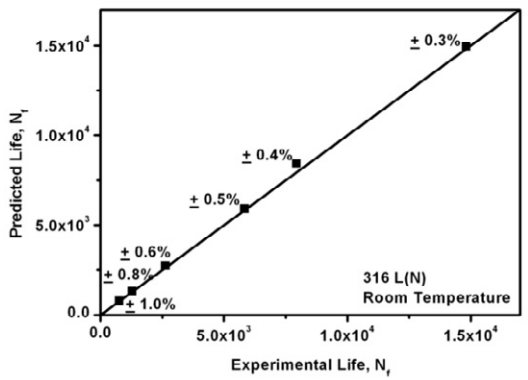

Fig. 8. LCF life prediction based on plastic strain energy dissipation by non-Masing analysis.

5. Conclusions

- Cyclic stress response of the material was characterized by initial hardening followed by prolonged softening, saturation and final failure.
- The material showed Masing behavior at low strain amplitudes and non-Masing behavior at higher strain amplitudes.
- Predicted first cycle hysteresis loops from simulation showed good correlation with the experimental results and fatigue life predicted by non-Masing analysis was found to be close to the actual fatigue life.

Acknowledgement

The authors are grateful to Shri S. C. Chetal, Director, IGCAR and Dr. T. Jayakumar, Director, Metallurgy and Materials Group, IGCAR for their constant encouragement and support. The authors are also thankful to Dr. A. K. Bhaduri, AD, MDTG and Dr. M. D. Mathew, Head, MMD for their keen interest in this work. Help rendered by Mr. K. Mariappan during the course of experimental work is greatly acknowledged.

References

[1] M.Valsan, A.Nagesha, K.B.S.Rao, S.L.Mannan, A comparative evaluation of low cycle fatigue and creep-fatigue interaction behaviour of 316L(N) stainless steel, 316 weld metal and 316L(N)/316 weld joint at 873K. *Trans. Ind. Inst. Metals* 53(2000)263-271.
[2] V.S.Srinivasan, M.Valsan, R.Sandhya, K.B.S.Rao, S.L.Mannan and D.H.Sastry, High temperature time dependent low cycle fatigue behaviour of a type 316 L(N) stainless steel. *Int. J. Fatigue* 21(1999)11-21.
[3] D.Lefebvre, F.Ellyin, Cyclic response and inelastic strain energy in low cycle fatigue. *Int. J. Fatigue* 6(1984)9-15.
[4] H.Mughrabi, H.-J.Christ, Cyclic deformation and fatigue of selected ferritic and austenitic steels-specific aspects. *ISIJ International* 37(1997)1154-1169.
[5] A.Plumtree, H.A.Abdel-Raouf, Cyclic stress-strain response and substructure. *Int. J. Fatigue* 23(2001)799-805.
[6] S.Sivaprasad, S.K.Paul, A.Das, N.Narasiah, S.Tarafder, Cyclic plastic behaviour of primary heat transport piping materials: Influence of loading schemes on hysteresis loop. *Mater. Sci. and Engg. A* 527(2010)6858-6869.
[7] L.P.Borrego, L.M.Abreu, J.M.Costa and J.M.Ferreira. Analysis of low cycle fatigue in AlMgSi aluminium alloys. *Anales De Mecánica De La Fractura* 20(2003)179-184.
[8] J.L.Chaboche, Time-independent constitutive theories for cyclic plasticity. *Int. J. Plasticity* 2(1986)149-188.
[9] Fionn Dunne and Nik Petrinic, *Introduction to Computational Plasticity*, Oxford University Press, UK; 2005.